Spectrochimica Acta Part A: Molecular and Biomolecular Spectroscopy 255 (2021) 119686

Contents lists available at ScienceDirect

Spectrochimica Acta Part A: Molecular and Biomolecular Spectroscopy

journal homepage: www.elsevier.com/locate/saa

A red-emissive and positively charged RNA ligand enables visualization of mitochondrial depolarization and cell damage

Dingyi Guo [a], Jie Sun [a], Minggang Tian [a], Weiying Lin [a,b,*]

[a] Institute of Fluorescent Probes for Biological Imaging, School of Chemistry and Chemical Engineering, School of Materials Science and Engineering, University of Jinan, Jinan, Shandong 250022, PR China

[b] Guangxi Key Laboratory of Electrochemical Energy Materials, Institute of Optical Materials and Chemical Biology, School of Chemistry and Chemical Engineering, Guangxi University, Nanning, Guangxi 530004, PR China

HIGHLIGHTS

- A cationic red-emissive RNA ligand is constructed to detect mitochondrial depolarization.
- The probe targets mitochondria in live cells and migrates into nucleolus after loss of $\Delta\Psi_m$.
- Two cations are decorated on the probe which enables fast response to $\Delta\Psi_m$.
- Oxidative damage of live cells is clearly observed via subcellular immigration of the probe.

GRAPHICAL ABSTRACT

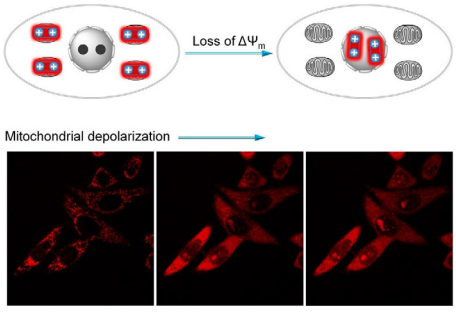

ARTICLE INFO

Article history:
Received 25 November 2020
Received in revised form 24 February 2021
Accepted 4 March 2021
Available online 10 March 2021

Keywords:
Fluorescent probe
Mitochondrial depolarization
RNA ligand
Mitochondria

ABSTRACT

In this work, a red-emissive RNA ligand bearing two positive charges were developed for the visualization of mitochondrial depolarization, via the subcellular localization of the ligand molecules. The ligand with quinolinium moiety and strong electronic donor displays red fluorescence peaked at 630 nm. Meanwhile, the probe is concentrated in mitochondria of live cells due to the high mitochondrial membrane potential, and re-localizes into nucleolus upon mitochondrial depolarization owing to the affinity to RNA. In this manner, the decrease of mitochondrial membrane potential could be *real-timely* and *in-situ* monitored with the red-emissive probe. Particularly, two cations were decorated on the probe, which enables the fast response to mitochondrial depolarization with elevated sensitivity. Cell damage induced by H_2O_2 was also successfully observed with the probe. We expect that the probe can promote researches on mitochondrial membrane potential, cell apoptosis, and relative areas.

1. Introduction

Mitochondrion is a crucial organelle in eukaryotic cells, which plays indispensable roles in providing intracellular energy, signalling, and many other biological events [1–3]. Particularly, aerobic respiration process occurs in mitochondrial inner membrane and matrix, during which two net protons were pumped out of mitochondria [4]. Therefore, a negatively inside transmembrane potential up to −180 mV is formed in mitochondria, namely the mitochondrial membrane potential ($\Delta\Psi_m$) [5,6]. $\Delta\Psi_m$ plays significant roles in the generation of ATP, signaling, and energy transition. Depolarization of $\Delta\Psi_m$ is an important sign of cell apoptosis, and also crucial for the signaling of autophagy process to control the quality of mitochondria in live cells [7–9]. Abnormal regulation of $\Delta\Psi_m$ is closely related to Alzheimer's disease, diabetes, cancer, and many other diseases [10–13]. Therefore, moni-

* Corresponding author.
E-mail address: weiyinglin2013@163.com (W. Lin).

https://doi.org/10.1016/j.saa.2021.119686
1386-1425/

toring $\Delta\Psi_m$ and visualizing mitochondrial depolarization are of fundamental significance for biology and pathology.

Determination of $\Delta\Psi_m$ had been a tough task in the past, because mitochondria exhibit small size (generally 1–3 μm) that is hard to insert an electrode [14]. The $\Delta\Psi_m$-dependent accumulation of membrane-permeable cations into mitochondria provided a valid way for assessment of $\Delta\Psi_m$ [15,16]. Fluorescent organic cations were utilized to monitor $\Delta\Psi_m$, in light of the superior advantages of fluorescence imaging technology, such as in-situ and real-time observation, high sensitivity, and low damages to biosamples [17–19]. Rhodamine dyes including tetramethylrhodamine (TMRM) and rhodamine 123 have been used for visualizing $\Delta\Psi_m$ under fluorescence microscopy [20,21]. The rhodamine dyes can light up mitochondria with high $\Delta\Psi_m$ in live cells, and the fluorescence significantly decreased during mitochondrial depolarization. Aggregation-induced emission (AIE) dyes were also exploited for visualization of $\Delta\Psi_m$ in *off–on* manner. Tang and co-workers have developed a positively changed and red-emissive AIEgen for visualizing $\Delta\Psi_m$, which displayed decreased emission in mitochondria upon mitochondrial depolarization [22]. Yoon's group has attached triphenylphosphonium to a green-emissive AIEgen, for detection of mitochondrial depolarization by reduced emission [23]. However, these probes might be interfered by many factors, such as the inhomogeneous distribution of probe molecules and fluctuation of equipment status.

To avoid the interferences, fluorescent probes with subcellular migration properties have been developed in recent years, for the visualization of mitochondrial depolarization. Yu's group has constructed a fluorescence DNA binder enabling migration from mitochondria to nucleus upon mitochondrial depolarization. Tian and co-workers have developed fluorescent Zinc complex which could migrate from mitochondria to nucleolus during the decrease of $\Delta\Psi_m$ [24]. Our group has also developed fluorescent probes capable of migration from mitochondria into nucleus/nucleolus with the decrease of $\Delta\Psi_m$ levels [17,25]. Recently, our group has reported a pH-sensitive RNA binder, which responsive to mitochondrial depolarization in ratiometric manner and via the subcellular immigration from mitochondria to nucleolus [26]. Moreover, we have also constructed a ratiometric probe visualizing mitochondrial depolarization based on intermolecular π-stacking interactions [27]. Yet, red-emissive fluorescent probes enabling $\Delta\Psi_m$-dependent subcellular migration from mitochondria into nucleus/nucleolus were still rarely reported. Since red-emissive probes for bioimaging applications display unique advantages including low interferences from endogenous fluorophores (typically ~450 nm from NADH in animal cells) [28], low photo-toxicity, and high penetration depth. Therefore, it is an urgent task to develop red-emissive fluorescent probes with subcellular migration properties for the visualization of mitochondrial depolarization.

2. Experimental section

Synthesis of 4,4′-(piperazine-1,4-diyl)dibenzaldehyde (**1**). Piperazine (10 mmol) was added into 40 mL methoxyethanol in a flask, which was stirred for 10 min to mix evenly. Then p-fluorobenzaldehyde (30 mmol) was dropped in, and the reactant was refluxed for 24 h to finish the reaction. After cooled down to room temperature, the mixture was mixed with 300 mL water and extract with 300 mL dichloromethane twice. The dichloromethane layer was dried with anhydrous magnesium sulfate and distilled in a rotary evaporator. The product was obtained by column chromatography and presented in light yellow powder (Yield, 36%). ^{1}H NMR (400 MHz, DMSO d_6) δ 9.74 (s, 2H), 7.97–7.48 (m, 4H), 7.26–6.72 (m, 4H), 3.61 (s, 8H).

Synthesis of 2,2′-((1E,1′E)-(piperazine-1,4-diylbis(4,1-phenylene))bis(ethene-2,1-diyl))bis(1-methylquinolin-1-ium) iodide (**DPEI**). The compound 2 was synthesized according to our previous report. Compound 1 (1 mmol) and 2 (3 mmol) was added into 8 mL ethanol in a round-bottom flask, which was stirred for more than 5 min to mix evenly. 3 drops of piperidine was added into the flask as catalyst, and the reactant was heated to reflux for 36 h. The system was cooled down to room temperature and there were solids precipitated. The solids were collected via filtration and obtained by column chromatography. The final product presented in brown powder (Yield, 41%). ^{1}H NMR (400 MHz, DMSO d_6) δ 8.90 (d, J = 9.0 Hz, 2H), 8.56 (d, J = 9.1 Hz, 2H), 8.49 (d, J = 9.0 Hz, 2H), 8.34–8.20 (m, 4H), 8.13 (t, J = 8.0 Hz, 2H), 7.92 (dd, J = 12.6, 8.1 Hz, 6H), 7.69 (d, J = 15.5 Hz, 2H), 7.14 (d, J = 8.6 Hz, 4H), 4.50 (s, 6H), 3.65 (s, 8H). ^{13}C NMR (101 MHz, DMSO) δ 179.18, 164.64, 147.88, 144.19, 143.14, 141.13, 139.87, 136.69, 135.97, 129.44, 128.19, 127.89, 124.63, 123.24, 118.95, 116.96, 114.20, 114.17, 112.13, 106.39, 51.28, 45.67, 27.29, 13.82, 8.83. HRMS (m/z): $[M]^{2+}$ calcd. for $C_{40}H_{38}N_4^{2+}$, 287.1543; found, 287.1543.

3. Results and discussion

3.1. Design and synthesis of the fluorescence probe

The immigration property was initially in consideration to design the fluorescent probe. To achieve the $\Delta\Psi_m$-dependent migration from mitochondria to nucleus/nucleolus, the probe should meet two criteria. Firstly, the probe should possess cationic groups to target mitochondria dependent on $\Delta\Psi_m$. Secondly, the probe should display suitable affinity to nucleic acids (NA), which ensures that the probe can move into nucleus/nucleolus after mitochondrial depolarization. Based on the two considerations, methyl quinolinium group was selected as the targeting group. The positive charge can drive the probe into mitochondria in live cells. The quinolinium group with short sidechain may afford high affinity to NA by binding to the grooves.

Aniline group with strong electronic donating property was selected to construct the other part of the probe. The strong electronic donor and acceptor endow probe **DPEI** a D-π-A electronic structure with long-wavelength emission. The probe was synthesized based on the synthetic route shown in Scheme 1b, and the synthesis procedures and characterizations were presented in the Experimental Section and supporting information.

3.2. Optical properties of the probe

The optical spectra of the probe, including absorption and emission spectra in different solvents, were acquired initially as depicted in Fig. 1. As demonstrated in Fig. 1a, the probe displayed absorption in the range from 400 nm to 650 nm, with absorption peaks around 500 nm in most solvents, and 550 nm in dichloromethane (DCM). The longer absorption in DCM should be resulted from the halogen bond. Meanwhile, in Fig. 1b **DPEI** showed emission in the range of 550–750 nm with the fluorescence peak around 630 nm, demonstrating the red-emissive property of the probe in various solvents. It should be noted that the probe presented evidently enhanced emission in glycerol with high viscosity, indicating that **DPEI** was sensitive to environmental viscosity. To demonstrate the viscosity-sensitive fluorescence of the probe, the emission spectra of **DPEI** in mixed solvent of glycerol and ethanol were obtained. As demonstrated in the Fig. S1, with the increase of glycerol fraction and viscosity, the fluorescence of **DPEI** steadily enhanced. Density functional theory (DFT) calculation was thereafter performed, to understand its response to environmental viscosity. As shown in Scheme 1a, the electron density in the ani-

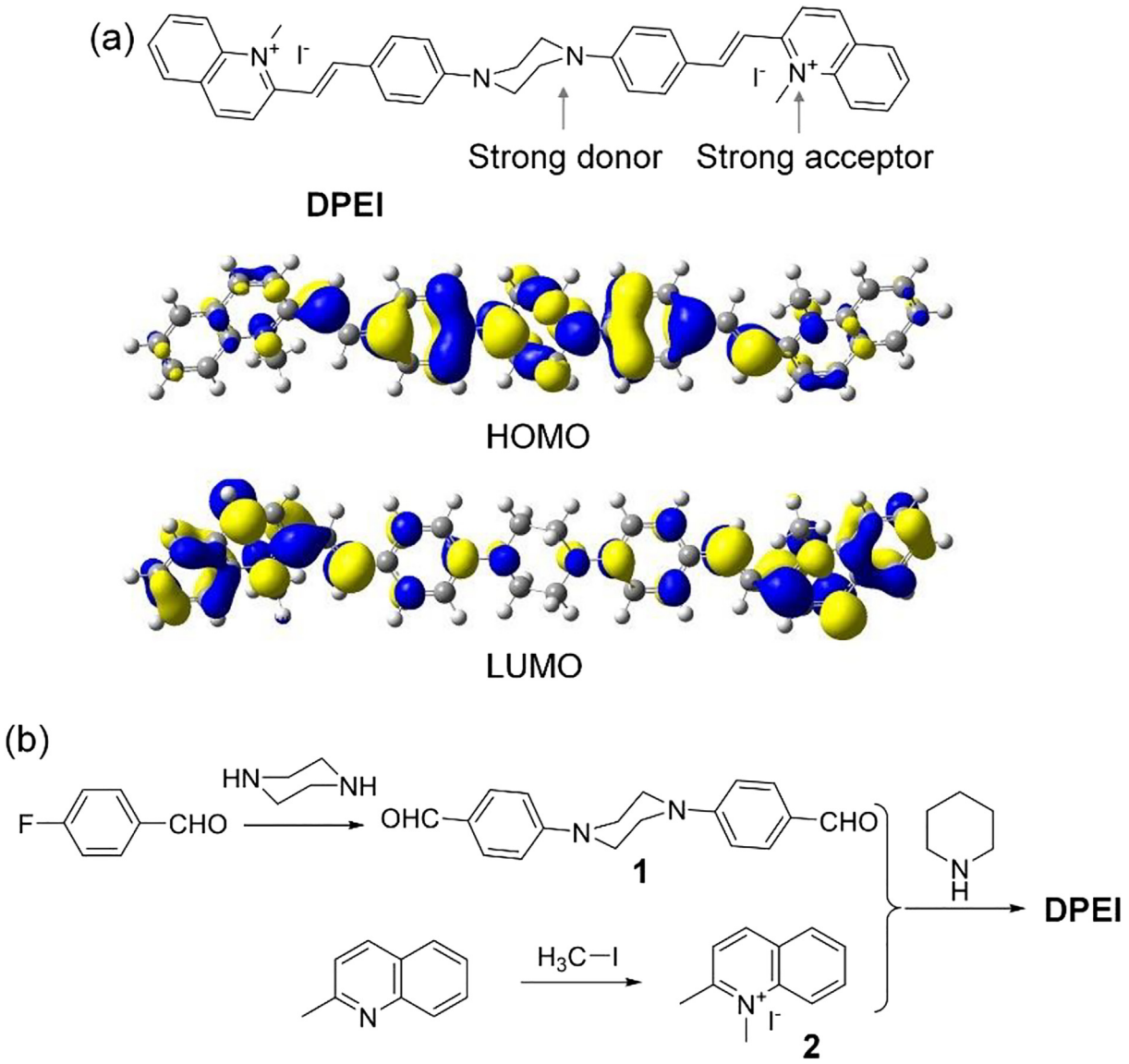

Scheme 1. (a) The chemical structure and frontier orbitals of probe **DPEI**; (b) The synthetic route of **DPEI**.

line moiety was higher than the quinolinium part in HOMO, while the electron density in aniline moiety was lower in LUMO. These results indicated the charge transfer from aniline moiety to quinolinium group during excitation. The intramolecular charge transfer (ICT) process in **DPEI** may cause the intramolecular motion, which should be responsible for the weak emission in low-viscosity solvents. In glycerol with high viscosity, the intramolecular motions could be restricted, which can recover the fluorescence.

Since the probe **DPEI** was expected to be a NA ligand that displayed high affinity to NA. The fluorescence of the probe in the presence of DNA and RNA was then testified. As shown in Fig. 1a, **DPEI** displayed decreased absorbance and slightly blue-shifted absorption in aqueous conditions. Meanwhile, as shown in Fig. 1b–d, the probe displayed very weak and red-shifted emission peaked around 720 nm in buffer solutions. These optical characters were in accordance with the H-aggregation, implying that **DPEI** might form H-aggregates in aqueous solutions. After the introduction of DNA/RNA, the probe could bind to DNA/RNA and form monomers, which may cause the fluorescence enhancement. Moreover, as demonstrated above, **DPEI** exhibited evidently enhanced emission in high-viscose conditions, due to the inhibition of intramolecular motions. The bind of DPEI to DNA/RNA might also inhibit the intramolecular motions and brought fluorescence enhancement.

Cytotoxicity of DPEI. To check the biocompatibility of **DPEI**, the cytotoxicity of the probe was evaluated via (3-(4,5-dimethylthiazol-2-yl)-2,5-diphenyltetrazolium bromide (MTT) assay. As illustrated in Fig. S2, after incubation by 2 μM DPEI for 2 h, 24 h, and 36 h, the cell viability of live HeLa cells was 0.995, 0.981, and 0.952, respectively. These results demonstrated ignorable cytotoxicity and high biocompatibility of probe **DPEI**, which was thus suitable for bioimaging experiments.

3.3. Different localizations of the probe in live and dead cells

Live HeLa cells were incubated with the probe, and cell images were obtained by confocal microscope. As shown in Fig. 2, the fluorescent signals of **DPEI** were localized in extra-nuclear space of live cells, and imaged as filament morphologies. These results demonstrated that **DPEI** might stain mitochondria of live cells

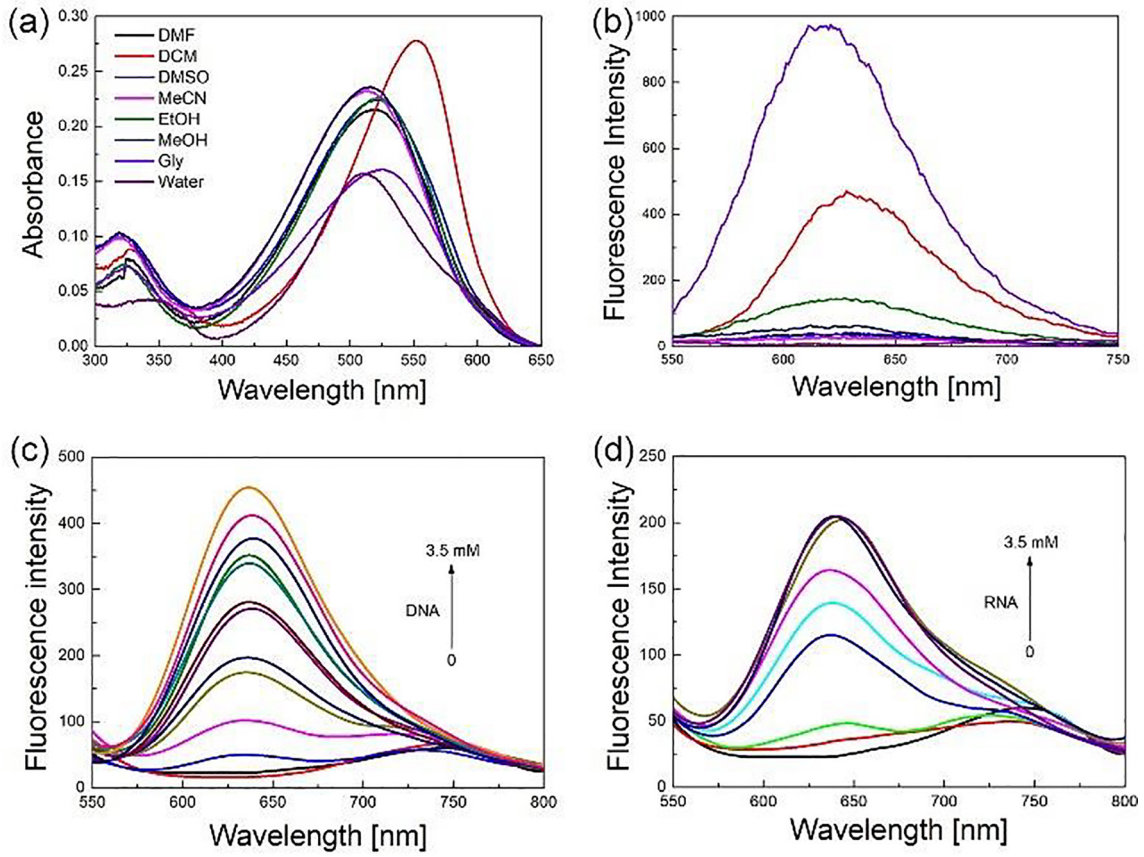

Fig. 1. The absorption (a) and fluorescence (b) spectra of 5 μM probe **DPEI** in various solvents; the emission spectra of 5 μM probe **DPEI** in different concentration of DNA (c) and RNA (d). Excitation wavelength: 500 nm; slit width: 5.0 for excitation, 5.0 for emission collection.

because of high $\Delta\Psi_m$. The $\Delta\Psi_m$ was completely depolarized in fixed cells, and consequently HeLa cells were fixed by paraformaldehyde and incubated by the probe. As shown in Fig. 2, the probe targeted nucleolus and cytoplasm in fixed cells. The obviously different localizations of **DPEI** in live and dead cells could be used to monitor the mitochondrial depolarization. The localization in nucleolus in fixed cells may be attributed to the affinity of **DPEI** to NA, as illustrated in Fig. 1c and d. Since almost all of the DNA distributed in the nucleus in eukaryotic cells, while the RNA distributed in nucleolus and cytoplasm, **DPEI** may bind to intracellular RNA in fixed cells. To clarify the targets of DPEI in fixed cells, DNA and RNA digestion experiments have been carried out as shown in Fig. S3. As shown in the figure, **DPEI** showed intense emission in cytoplasm and nucleolus in fixed cells. After the treatment of DNase and the digestion of DNA, the fluorescence slightly decreased. By contrast, By contrast, after the treatment of RNase and the digestion of RNA, the intracellular emission evidently decreased. Thus, the probe should bind to RNA in fixed cells, and the localization of the probe in nucleolus should be attributed to its affinity to RNA.

Colocalization experiments was then used to confirm the location of the probe in live cells. MitoTracker deep-red (MTDR), a commercialized mitochondrial probe, was selected for co-localization experiments. The fluorescence of MTDR could not excited by 488 nm, while the probe **DPEI** showed no absorption at 647 nm. Consequently, the fluorescence excited by 647 nm was from MTDR, while that excited by 488 nm was from **DPEI**. As illustrated in Fig. S4, the emission signal of **DPEI** overlapped well with that of MTDR, and the Pearson's co-localization coefficient was up to 0.92. The co-localization experiments further confirmed that **DPEI** targeted mitochondria in live cells.

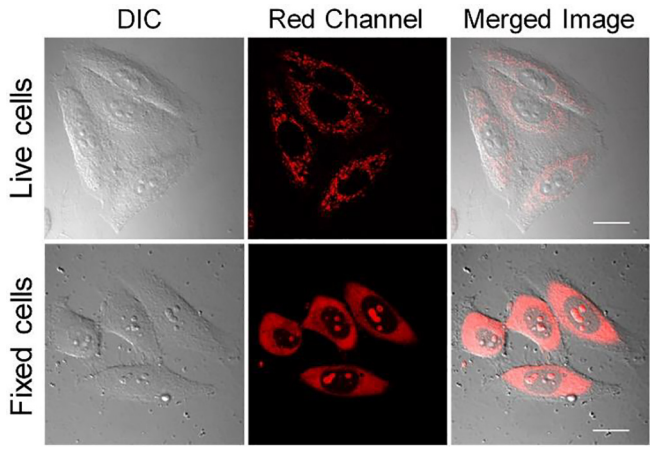

Fig. 2. The DIC and fluorescence images of live and dead HeLa cells incubated by 2 μM **DPEI** for 20 min. Excitation wavelength: 561 nm. Bar = 20 μm.

3.4. Monitoring mitochondrial depolarization from subcellular migration

As presented above, the probe **DPEI** was concentrated in mitochondria of live cells due to high $\Delta\Psi_m$, and distributed in nucleolus of dead cells with depolarized $\Delta\Psi_m$. Consequently, **DPEI** was potential to image the depolarization process of $\Delta\Psi_m$. Carbonyl cyanide 3-chlorophenylhydrazone (CCCP) is a kind of protonophore that can rapidly and efficiently induce mitochondrial depolarization. The possible effect of CCCP on the probe **DPEI** was

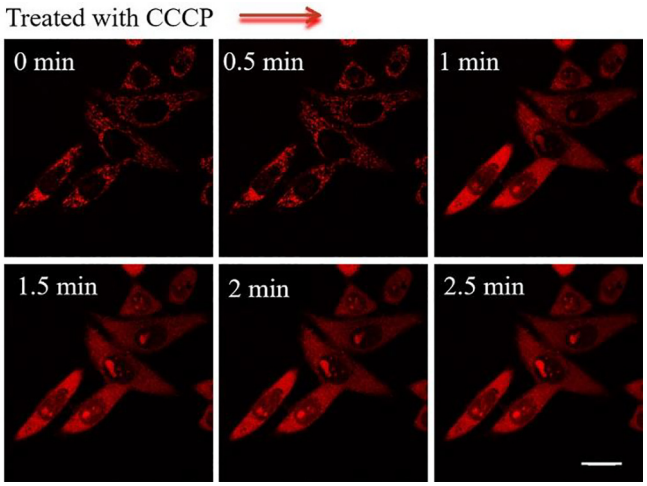

Fig. 3. The fluorescence images of HeLa cells pre-incubated by 2 μM **DPEI** for 20 min and then 10 μM CCCP was added to depolarized mitochondria. Bar = 20 μm.

firstly assessed via fluorescence spectroscopy. As shown in Fig. S5, Obviously, the addition of CCCP would not affect the fluorescence of DPEI, indicating ignorable interactions between CCCP and **DPEI**. Moreover, to prove that CCCP can actually depolarize the mitochondria, live HeLa cells were incubated by JC-1, a commercialized fluorescent probe to detect $\Delta\Psi_m$. As shown in Fig. S6, bright green and red fluorescence could be observed in live cells incubated by JC-1. After the addition of 10 μM CCCP for 5 min, the green emission increased while the red fluorescence decreased. These results demonstrated that JC-1 can cause the rapid decrease of $\Delta\Psi_m$ in live cells. Live HeLa cells were pre-incubated by probe **DPEI** and then treated by CCCP. As shown in Fig. 3, **DPEI** targeted mitochondria in cells with the high levels of $\Delta\Psi_m$, and presented in filament morphologies. After the addition of 10 μM CCCP the $\Delta\Psi_m$ was gradually depolarized, and the **DPEI** molecules moved out of mitochondria and migrated into the nucleolus. Within 2.0–2.5 min, the filament morphologies in cytoplasm disappears, and the emission in nucleolus became intense. These results demonstrate that **DPEI** could image the depolarization of $\Delta\Psi_m$ with high sensitivity.

3.5. Monitor oxidative damage by H_2O_2

Hydrogen peroxide (H_2O_2) is a kind of reactive oxygen species, and also an important byproduct of respiration reaction·H_2O_2 can bring severe oxidative damage to live cells and cause the mitochondrial depolarization. The possible interaction between H_2O_2 and **DPEI** was also testified using fluorescence spectra as shown in Fig. S5. The figure demonstrated that 10 mM H_2O_2 would not bring significant emission change of **DPEI**, indicating that the interaction between H_2O_2 and **DPEI** could be ignored. Consequently, live HeLa cells were pre-incubated by the probe **DPEI**, and then treated with H_2O_2. As presented in Fig. 4, the probe **DPEI** stained mitochondria of live cells. After the introduction of H_2O_2, the fluorescence in mitochondria gradually faded, and the nucleolus was steadily lighted up by intense emission. The change of probe localization indicating the depolarization of $\Delta\Psi_m$ induced by oxidative damage. Therefore, the oxidative damage of HeLa cells induced by H_2O_2 could monitored by the probe.

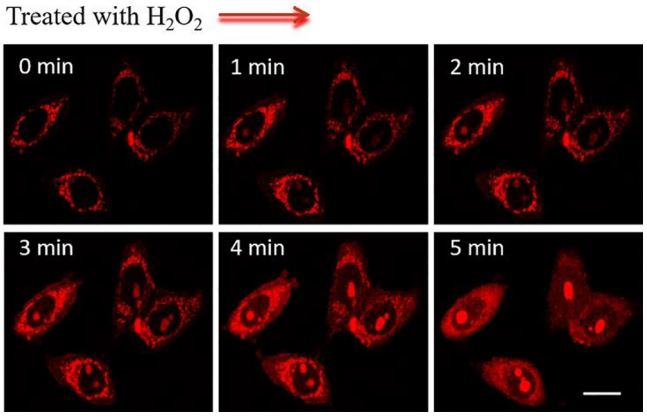

Fig. 4. The fluorescence images of HeLa cells incubated by 2 μM **DPEI** for 20 min and then 5 mM H_2O_2 was used to induce the oxidative damages. Bar = 20 μm.

4. Conclusion

In summary, a red-emissive probe that can migrate from mitochondria to nucleolus during mitochondrial depolarization was fabricated in this work. The probe exhibited a D-π-A electronic structure, and displayed red emission peaked around 630 nm. Meanwhile, the probe exhibited two positive charges and showed high affinity to NA. As a result, the probe targeted mitochondria in live cells with high $\Delta\Psi_m$, and immigrated into nucleolus upon mitochondrial depolarization. Consequently, mitochondrial depolarization could be efficiently monitored by the subcellular immigration of the probe with high sensitivity. Particularly, the probe displayed duple cationic groups and thus showed fast response to mitochondrial depolarization with evidently elevated sensitivity. Oxidative damage by H_2O_2 to live cells was also successfully monitored by the probe. Therefore, this red-emissive probe for mitochondrial depolarization could be utilized to visualize $\Delta\Psi_m$, detect cell damage, and promote researches in relative areas.

CRediT authorship contribution statement

Dingyi Guo: Methodology, Visualization, Investigation. **Jie Sun:** Methodology, Visualization, Investigation. **Minggang Tian:** Conceptualization, Validation, Writing - review & editing. **Weiying Lin:** Conceptualization, Validation, Writing - review & editing.

Declaration of Competing Interest

The authors declare that they have no known competing financial interests or personal relationships that could have appeared to influence the work reported in this paper.

Acknowledgements

For financial support, we thank the National Natural Science Foundation of China (NSFC) (21672083, 21877048, 21804052, 22077048), the Taishan Scholar Foundation (TS201511041), the Natural Science Foundation of Shandong Province (ZR2018BB058), and the startup funds of University of Jinan (309-10004, 160100331).

Appendix A. Supplementary material

Supplementary data to this article can be found online at https://doi.org/10.1016/j.saa.2021.119686.

References

[1] D. Acuña-Castroviejo, M. Martín, M. Macías, G. Escames, J. León, H. Khaldy, R.J. Reiter, Melatonin, mitochondria, and cellular bioenergetics, J. Pineal Res. 30 (2001) 65–74.
[2] J. Sastre, F.V. Pallardó, J. García de la Asunción, J. Viña, Mitochondria, oxidative stress and aging, Free Radical Res. 32 (2000) 189–198.
[3] H.M. McBride, M. Neuspiel, S. Wasiak, Mitochondria: more than just a powerhouse, Curr. Biol. 16 (2006) R551–R560.

[4] H. Vakifahmetoglu-Norberg, A.T. Ouchida, E. Norberg, The role of mitochondria in metabolism and cell death, Biochem. Biophys. Res. Commun. 482 (2017) 426–431.
[5] L.B. Chen, Mitochondrial membrane potential in living cells, Ann. Rev. Cell Biol. 4 (1988) 155–181.
[6] L.D. Zorova, V.A. Popkov, E.Y. Plotnikov, D.N. Silachev, I.B. Pevzner, S.S. Jankauskas, V.A. Babenko, S.D. Zorov, A.V. Balakireva, M. Juhaszova, S.J. Sollott, D.B. Zorov, Mitochondrial membrane potential, Anal. Biochem. 552 (2018) 50–59.
[7] C. Wang, R.J. Youle, The role of mitochondria in apoptosis, Ann. Rev. Genet. 43 (2009) 95–118.
[8] B. Mignotte, J.-L. Vayssiere, Mitochondria and apoptosis, Eur. J. Biochem. 252 (1998) 1–15.
[9] K. Wang, D.J. Klionsky, Mitochondria removal by autophagy, Autophagy 7 (2011) 297–300.
[10] J. Long, P. He, Y. Shen, R. Li, New evidence of mitochondria dysfunction in the female Alzheimer's disease brain: deficiency of estrogen receptor-β, J. Alzheim. Dis. 30 (2012) 545–558.
[11] M. Hüttemann, I. Lee, A. Pecinova, P. Pecina, K. Przyklenk, J.W. Doan, Regulation of oxidative phosphorylation, the mitochondrial membrane potential, and their role in human disease, J. Bioenerg. Biomembr. 40 (2008) 445.
[12] B. Kadenbach, R. Ramzan, R. Moosdorf, S. Vogt, The role of mitochondrial membrane potential in ischemic heart failure, Mitochondrion 11 (2011) 700–706.
[13] P. Bullon, M.D. Cordero, J.L. Quiles, J.M. Morillo, M. del Carmen Ramirez-Tortosa, M. Battino, Mitochondrial dysfunction promoted by Porphyromonas gingivalis lipopolysaccharide as a possible link between cardiovascular disease and periodontitis, Free Radical Biol. Med. 50 (2011) 1336–1343.
[14] L. Ernster, G. Schatz, Mitochondria: a historical review, J. Cell Biol. 91 (1981) 227s–255s.
[15] H. Steen, J.G. Maring, D.K. Meijer, Differential effects of metabolic inhibitors on cellular and mitochondrial uptake of organic cations in rat liver, Biochem. Pharmacol. 45 (1993) 809–818.
[16] K.S. Rogers, E.S. Higgins, Lipophilic interactions of organic cations with mitochondrial inner membranes during respiratory control, J. Biol. Chem. 248 (1973) 7142–7148.
[17] M. Tian, J. Sun, B. Dong, W. Lin, Dynamically monitoring cell viability in a dual-color mode: construction of an aggregation/monomer-based probe capable of reversible mitochondria-nucleus migration, Angew. Chem. Int. Ed. 57 (2018) 16506–16510.
[18] M. Tian, Y. Ma, W. Lin, Fluorescent probes for the visualization of cell viability, Acc. Chem. Res. 52 (2019) 2147–2157.
[19] H. Chen, B. Dong, Y. Tang, W. Lin, A unique "integration" strategy for the rational design of optically tunable near-infrared fluorophores, Acc. Chem. Res. 50 (2017) 1410–1422.
[20] A. Baracca, G. Sgarbi, G. Solaini, G. Lenaz, Rhodamine 123 as a probe of mitochondrial membrane potential: evaluation of proton flux through F0 during ATP synthesis, BBA-Bioenergetics 1606 (2003) 137–146.
[21] R.C. Scaduto Jr, L.W. Grotyohann, Measurement of mitochondrial membrane potential using fluorescent rhodamine derivatives, Biophys. J. 76 (1999) 469–477.
[22] N. Zhao, S. Chen, Y. Hong, B.Z. Tang, A red emitting mitochondria-targeted AIE probe as an indicator for membrane potential and mouse sperm activity, Chem. Commun. 51 (2015) 13599–13602.
[23] J. Li, N. Kwon, Y. Jeong, S. Lee, G. Kim, J. Yoon, Aggregation-induced fluorescence probe for monitoring membrane potential changes in mitochondria, ACS Appl. Mater. Interfaces 10 (2017) 12150–12154.
[24] D. Liu, M. Zhang, W. Du, L. Hu, F. Li, X. Tian, A. Wang, Q. Zhang, Z. Zhang, J. Wu, A series of Zn (II) terpyridine-based nitrate complexes as two-photon fluorescent probe for identifying apoptotic and living cells via subcellular immigration, Inorg. Chem. 57 (2018) 7676–7683.
[25] M. Tian, J. Sun, B. Dong, W. Lin, Construction of mitochondria-nucleolus shuttling fluorescent probe for the reversible detection of mitochondrial membrane potential, Sensor. Actuator. B 292 (2019) 16–23.
[26] M. Tian, J. Sun, B. Dong, W. Lin, Unique pH-sensitive RNA binder for ratiometric visualization of cell apoptosis, Anal. Chem. 91 (2019) 10056–10063.
[27] M. Tian, J. Sun, B. Dong, Y. Ma, W. Lin, Dual-emissive probe for reversible visualization of $\Delta\Psi_m$ revealing voltage heterogeneity in a single mitochondrion, Anal. Chem. (2021), https://doi.org/10.1021/acs.analchem.0c04819.
[28] C. Ince, J. Coremans, H. Bruining, In vivo NADH fluorescence, Oxygen Transport Tissue XIV 317 (1992) 277–296.